Title

Scalable manufacturing of quantum light emitters in silicon under rapid thermal annealing.

Journal

Optics Express, 31(5)

ISSN

1094-4087

Authors

Zhiyenbayev, Yertay

Redjem, Walid

Ivanov, Vsevolod

et al.

Publication Date

2023-02-27

DOI

10.1364/oe.482311

Research Article | Vol. 31, No. 5 / 27 Feb 2023 / Optics Express 8352
Optics EXPRESS

Scalable manufacturing of quantum light emitters in silicon under rapid thermal annealing

YERTAY ZHIYENBAYEV,[1] WALID REDJEM,[1] VSEVOLOD IVANOV,[2,3] WAYESH QARONY,[1] CHRISTOS PAPAPANOS,[1] JACOPO SIMONI,[2] WEI LIU,[3] KAUSHALYA JHURIA,[3] LIANG Z. TAN,[2] THOMAS SCHENKEL,[3] AND BOUBACAR KANTÉ[1,4,*]

[1]*Department of Electrical Engineering and Computer Sciences, University of California, Berkeley, California 94720, USA*
[2]*Molecular Foundry, Lawrence Berkeley National Laboratory, Berkeley, California 94720, USA*
[3]*Accelerator Technology and Applied Physics Division, Lawrence Berkeley National Laboratory, Berkeley, California 94720, USA*
[4]*Materials Sciences Division, Lawrence Berkeley National Laboratory, Berkeley, CA, USA*
[*]*bkante@berkeley.edu*

Abstract: Quantum light sources play a fundamental role in quantum technologies ranging from quantum networking to quantum sensing and computation. The development of these technologies requires scalable platforms, and the recent discovery of quantum light sources in silicon represents an exciting and promising prospect for scalability. The usual process for creating color centers in silicon involves carbon implantation into silicon, followed by rapid thermal annealing. However, the dependence of critical optical properties, such as the inhomogeneous broadening, the density, and the signal-to-background ratio, on centers implantation steps is poorly understood. We investigate the role of rapid thermal annealing on the dynamic of the formation of single color centers in silicon. We find that the density and the inhomogeneous broadening greatly depend on the annealing time. We attribute the observations to nanoscale thermal processes occurring around single centers and leading to local strain fluctuations. Our experimental observation is supported by theoretical modeling based on first principles calculations. The results indicate that annealing is currently the main step limiting the scalable manufacturing of color centers in silicon.

1. Introduction

Perfect crystals do not exist owing to the presence of inherent defects. Most crystalline defects are undesirable in silicon wafers. However, certain types of defects such as straight dislocations, stacking faults, and extrinsic dopants are essential for microelectronics and optoelectronic devices [1–8]. Luminescent atomic defects, or color-centers, also show great potential for solid state-based quantum technologies because they can mimic the optoelectronic properties of an embedded single atom [9,10]. The G-center is the most well-known luminescent atomic defect in silicon, first measured in 1968 after electron irradiation of silicon [11]. It is composed of two carbon atoms bound to the same silicon self-interstitial [12–20]. The G-center was the first to be isolated [21,22] because it has the largest oscillator strength among color-centers in silicon and a short (nanosecond) decay time [17,23]. The W and T centers were isolated afterwards [24–26]. More recently, a single spin in silicon has been observed optically and the integration of a single center in a silicon waveguide was reported [26,27]. However, despite important progress, the scalability of classical and quantum light sources is still a challenging question [28,29]. The inhomogeneous broadening of approximately 15 nm in the zero-phonon-line of single centers [21] compared to the broadening for an ensemble (0.3 nm) [17,30], the signal-to-background

#482311 https://doi.org/10.1364/OE.482311
Journal © 2023 Received 30 Nov 2022; revised 29 Jan 2023; accepted 7 Feb 2023; published 21 Feb 2023

Optics EXPRESS

ratio, cause challenges to the indistinguishability of photons originating from distinct centers [31].

The fabrication process of single centers consists of two main steps. The first step involves the implantation of carbon to increase carbon density within the silicon matrix and the second step involves rapid thermal annealing to cure the crystal [32–34]. We investigate the role of rapid thermal annealing on the dynamic of the formation of single-color centers in silicon. We find that the density of centers decreases exponentially with the annealing time. We also observe that the inhomogeneous broadening dramatically depends on the annealing time and can be decreased by a factor of three compared to the current practice. We attribute the observations to nanoscale thermal processes occurring around single centers and leading to local strain fluctuations. This work shows that while annealing is critical for the formation of single color-centers, it also constitutes the current limiting factor for the large-scale synthesis of single artificial atoms in silicon.

2. Silicon implantation and experimental setup

Figure 1(a) presents a commercial 230 nm float-zone SOI wafer that is carbon implanted at 36 keV at a fluence of $5 \times 10^{13}\,\mathrm{cm}^{-2}$ to increase the concentration of carbon in the middle of the silicon layer at a depth of about 100 nm. An ensemble of G-centers is formed as shown in Fig. 1(b). After cleaning, the carbon implanted sample was annealed using a rapid thermal processor with controllable annealing time and temperature. The annealing in Fig. 1(c) was performed under

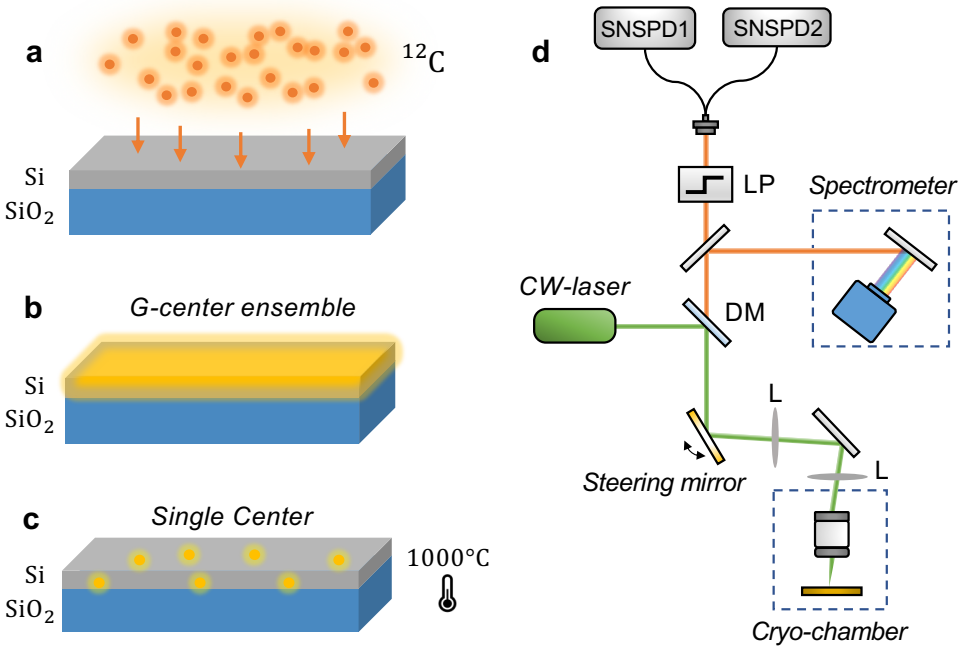

Fig. 1. Implantation process of color centers in silicon and characterization setup. (a-c) The fabrication process uses a standard commercial SOI wafer that is implanted with carbon at 36 keV at a fluence of $5 \times 10^{13}\,\mathrm{cm}^{-2}$(a). The implantation results in the formation of a G-center ensemble in the middle of Si-layer (b). The creation of single color-centers involves rapid thermal annealing under controlled conditions (c). Characterization setup to detect the luminescence of single centers in silicon. SNSPD: superconducting nanowire single-photon detector. CW-laser: continuous-wave laser. LP: long pass filter. DM: dichroic mirror. L: lens (d).

Optics EXPRESS

nitrogen (N_2), an inert gas, to create color centers. A rigorous control profile with rapid ramp-up and ramp-down was used to achieve the target temperature for a short duration that is significant for the damage-repairing process caused by the ion implantation. The rate of temperature rise was 275 °C per second, while the cooling was performed at a rate of 85 °C per second.

The annealing time was varied from 3 to 50 seconds in our work, with distinct samples being used for each annealing time. Figure 1(d) presents the optical measurements setup, a home-built confocal photo-luminescence microscope operating at 5 K. A continuous-wave (CW) laser beam at 532 nm was used to pump the sample with a power of 0.3 mW. A dichroic mirror and an additional long-pass filter separated the signal from the pump beam. Integrated photoluminescence (PL) from 1200 to 1600 nm was collected using a superconducting single-photon detector (SNSPD) with a system detection efficiency of 85% at 1310 nm. To measure second-order auto-correlation, we used a Hanbury-Brown and Twiss interferometer that consists of two SNSPDs and a fiber beam splitter. The detectors, in combination with a steering mirror, were utilized to make fine-raster scans of the samples. Finally, the photoluminescence spectrum was recorded with an InGaAs camera at the exit of a grating spectrometer with a resolution of 0.28 nm.

3. Results

3.1. Annealing dependent dynamic of the formation of color-centers

Photoluminescence (PL) raster scans of the sample before implantation, after implantation, and after annealing are presented in Fig. 2. Typically, a vintage sample (before annealing) does not contain any color centers, and this is confirmed by the PL shown in Fig. 2(a). After carbon (C) implantation, Fig. 2(b) shows a strong PL signal compared to the non-implanted sample. The relatively uniform signal over the sample corresponds to an ensemble of G-centers with a spectrum shown in black in Fig. 2(d). During implantation a high concentration of $C_{(i)}$ is generated through the direct incorporation of the carbon into the silicon lattice, and through the formation of silicon self-interstitials, $Si_{(i)}$, which can replace substitutional carbons, $C_{(s)}$ in the lattice to create $C_{(i)}$. The created $C_{(i)}$ is highly mobile, moving relatively freely throughout the lattice until it is captured by another $C_{(s)}$ elsewhere in the silicon structure [17,35,36]. This intermediate (CC) center then undergoes a structural rearrangement to become the bright B-form of the G-center (GCB) composed of two $C_{(s)}$ and an interstitial $Si_{(i)}$ [36]. The process of implantation and creation of ensemble of G-centers, although well established, will be particularly relevant to understand the creation and quality of single centers upon annealing.

Figure 2(c) shows diffraction-limited spots measured after the rapid thermal annealing step at 1000°C for 20 seconds. The inset shows a magnified region containing a single defect. The spectrum of the defect is shown in Fig. 2(d) (red color). We observe a detuning between the zero-phonon lines (ZPLs) of the single center and the ensemble. The full peak width at half maximum (FWHM) of the single G-center is limited by the resolution of the grating (0.28 nm), while the FWHM of the ensemble is 0.88 nm. The larger FWHM of the ensemble compared to the literature [23] originates from the carbon implantation that causes more atomic disorder than proton irradiation [37]. Second-order auto-correlation measurements confirmed that the emission is from a single emitter. The anti-bunching effect can be seen in Fig. 2(e) where $g^2_{\mathrm{exp}}(0) \approx 0.27 \pm 0.08$. The much smaller jitter of the SNSPDs (25 ps) compared to the relaxation dynamics of the center (30 ns) causes the background signal to limit the value of the antibunching at zero-delay [21]. We estimate the signal-to-background ratio (SBR) γ, by: $\gamma = S/(S+B)$, where S is the collected PL signal when pumping the defect and B is the measured background PL when the laser is pumping a neighboring region at about ±2 μm away from the defect. From measurements of the signal and background, the correction to the experimental value can be estimated from $g^{(2)}(\tau)$: $g_{\mathrm{cor}}{}^{(2)}(\tau) = [g_{\mathrm{exp}}{}^{(2)}(\tau)-(1-\gamma^2)]/\gamma^2$, where $g_{\mathrm{exp}}{}^{(2)}(\tau)$ are the normalized coincidence counts [38]. The signal-to-background ratio (SBR) from Fig. 2(e), is $\gamma = 0.85 \pm 0.02$ and the value matches well with the value at zero-delay of the anti-bunching $g_{\mathrm{exp}}{}^{(2)}(0)$. The purity

Optics EXPRESS

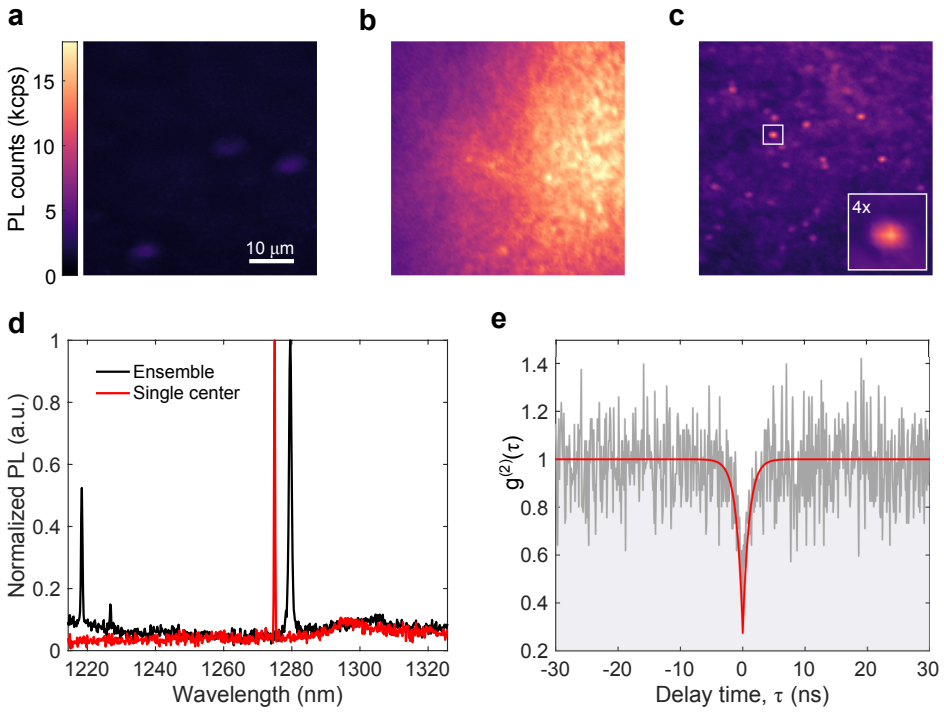

Fig. 2. Optical characterization of color centers in silicon. Photoluminescence (PL) raster scan of (a) non-implanted commercial SOI wafer, (b) SOI wafer after C-implantation, and (c) SOI wafer after annealing at 1000°C for 20 s. The inset in (c) shows a zoom-in image of a single color-center. (d) Spectra from an ensemble of G-centers (seen in b) and from a single center (seen in c). (e) Second order auto-correlation measurements exhibiting a clear anti-bunching at a zero-delay, proving the isolation of a single center.

of the single photon source can thus be quantified by the signal-to-background ratio (a quantity that is experimentally easier to measure). Each spot observed in the raster scan of Fig. 2(c) is assumed to be a single or a few emitters. This assumption is justified by the low density of defects and is further confirmed by the PL spectra of the defects.

3.2. *Temperature-dependent signal-to-background ratio and density of single color-centers*

To understand the effect of annealing on the formation of single centers, the PL signal of samples annealed from 5 seconds to 30 seconds at 1000°C was compared. In Figs. 3 and 4, we consider a defect as a single center based on the following characteristics: spatial isolation, pronounced sharp zero-phonon line (<0.3 nm) in the O-band and antibunching in the second-order correlation function. Figures 3(a)-(d) present the distribution of emitters as a function of the signal to background ratio (SBR), γ. A SBR value greater than 0.5 indicates that the emission originates from a single emitter. Other defects correspond to single centers, but their emission rate is comparable to the background photoluminescence and the value of the antibunching does not go below 0.5 (see Supplement 1). It is worth mentioning that the low SBR is unlikely to come from multiple emitters because the spectrum exhibits only a single sharp zero-phonon line. As the annealing time is increased from 5 s, 10 s, 20 s, to 30 s, the percentage of single emitters with a SBR (γ) larger than 0.5 increases from 24% to 40%. The relative percentage of spots corresponding to single photon sources increases with the annealing time. It is worth noting that

Optics EXPRESS

the photoluminescence counts of the isolated emitters do not depend on the annealing time. This indicates that the signal-to-background ratio is improving due to a decrease in the background signal with the annealing time (see Supplement 1).

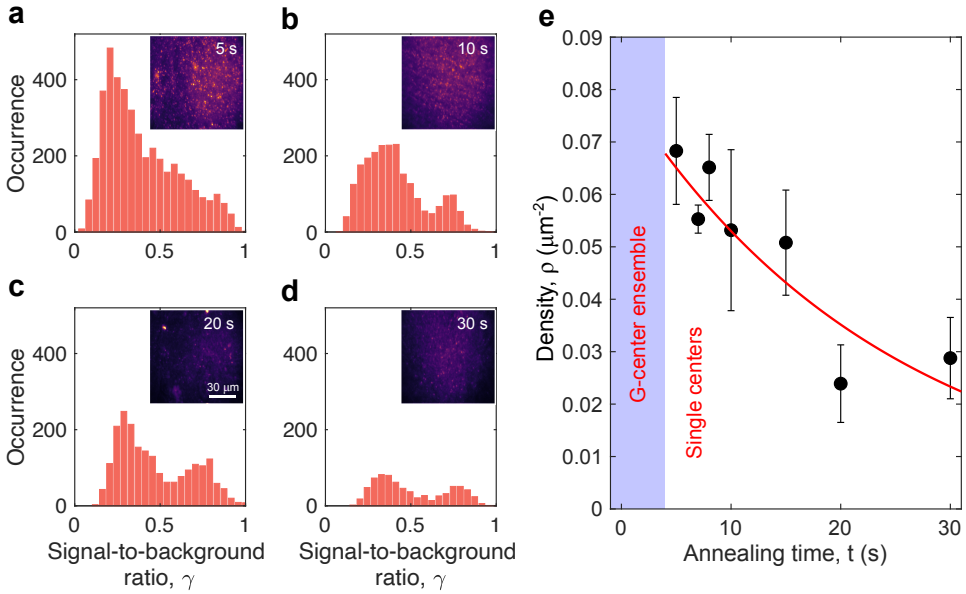

Fig. 3. Evolution of the density of single centers with the annealing time. Density distribution of single centers with respect to their signal-to-background ratio γ for annealing times of (a) 5 s, (b) 10 s, (c) 20 s, and (d) 30 s. The inset figures correspond to the PL raster scan. (e) Dependence of the density of single centers on the annealing time. The solid red line denotes an exponential fit. The error bars are determined by the standard deviation of the series of measurements performed in different locations of each sample. The region colored in blue shows the annealing times which favor ensembles of G-centers. The white region corresponds to the annealing time window that results in a formation of single color centers.

The origin of the background signal is difficult to identify because it has no distinct feature in the photoluminescence spectrum. It may correspond to optically inactive G-centers such as the A-form or other carbon/oxygen-related defects with no distinct zero phonon line. Thermal annealing can also introduce defects in addition to those created through implantation. For instance, oxygen or Si-vacancies may diffuse from the interface between silicon-air and silicon-buried oxide. To confirm this hypothesis, samples that did not go through the carbon-implantation step were annealed. We found that the average PL signal increases with annealing time, meaning that luminescent defects are incorporated through annealing. Compared to carbon-implanted samples, the PL signal is decreasing because of the rapid thermal destruction of the G-centers at 1000°C. For lower annealing temperatures, we observe a huge enhancement of the background signal for carbon-implanted samples, confirming that thermal annealing introduces defects. The improvement of the signal-to-background ratio is also accompanied by a decrease in the density of defects with the annealing time, as shown in Fig. 3(e). The density of single centers follows an exponential decay (solid red line in Fig. 3(e)): $\rho(t) = a \times e^{(-t/\tau)}$, with $a = 0.08 \pm 0.03\ \mu m^{-2}$ and an activation time of $\tau = 24.4 \pm 7.0$ s. The error bars in Fig. 3(e) are obtained by raster scanning the sample in various locations and computing a standard deviation. The current strategy using relatively high carbon implantation forms a high density of G-centers and annealing at high temperatures for a short time is necessary for observing single centers. The observation of single

Optics EXPRESS

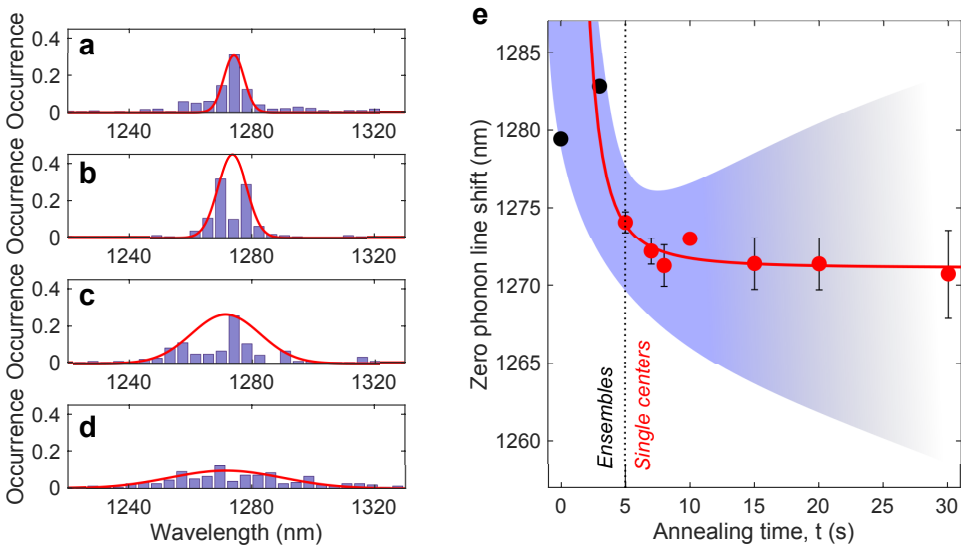

Fig. 4. Emission distribution of single color-centers. Distribution of the zero-phonon line (ZPL) wavelength for (a) 5 s (sample size is 584), (b) 10 s (sample size is 160), (c) 20 s (sample size is 181), and (d) 30 s (sample size is 157) of rapid thermal annealing. The solid red lines correspond to a Gaussian distribution fit. (e) Zero phonon line shift as a function of the thermal annealing time. The dashed line separates single centers from ensembles' thermal annealing regime. The solid red line corresponds to a phenomenological polynomial fit. The error bars in Fig. 4(e) correspond to the uncertainty in the gaussian fit of the ZPL distribution.

centers is made possible due to the exponential decrease of the density until the single-center density level is reached. We note that the highest density of 0.07 μm^{-2} was achieved for 5 s annealing. Annealing the sample for a shorter time led to an ensemble of G-centers. The maximum detected density of single centers is not limited by the resolution of the microscope but may be due to more complex phenomena such as electron-hole diffusion that limit the density of individually addressable single centers. The activation energy of $C_{(s)}$ and $Si_{(i)}$ is on the order of 4 eV, much larger than the thermal activation of $C_{(i)}$ which is 0.9 eV. At 1000°C the decrease in the density of centers is mainly due to the release of $C_{(i)}$ from the G-center. The G-centers would then attain a transition from the B-form consisting of two $C_{(s)}$ to the A-form that consists of one $C_{(s)}$ and one $C_{(i)}$. The $C_{(i)}$ is then released through a stochastic process. This is confirmed by the fact that the activation and migration energy of the $C_{(i)}$ is comparable to the thermal destruction energy of G-centers which is around 0.9 eV [39,40]. It is also worth noting that for annealing times greater than 30 s, all the single centers are dissolved. Upon annealing, C atoms escape toward the free surface of the sample [40–42] and cannot seed the formation of G-centers. The diffusion of carbon toward the surface is confirmed by the secondary ion mass spectrometry (SIMS) measurements of post-annealed carbon samples at 1000°C for the 20 s (see Supplement 1) where two maxima in the concentration of carbon at both the top and bottom interfaces are observed. After annealing, another implantation would be required to provide new $C_{(i)}$ to create new G-centers. The annealing time is thus critical and needs to be fine-tuned to form single centers.

3.3. *Inhomogeneous broadening of single centers*

Annealing at high temperatures causes distinct effects on the optical properties of single centers, especially with silicon color centers where the inhomogeneous broadening (15 nm) is fifty times

Optics EXPRESS

larger than the inhomogeneous broadening of an ensemble of G-centers (0.3 nm). We measured the spectrum for approximately 150 individual defects for each sample annealed from 5 s to 30 s. The distribution of the ZPL wavelength of the single emitter is reported in the histograms in Fig. 4(a)-(d). The ZPL wavelengths are well fitted by a gaussian distribution in red lines in Fig. 4(a)-(d). For the sample annealed for 5 s, most defects emit around 1274 nm with a standard deviation of 5.5 nm. For longer annealing time, the probability of emitting at a particular wavelength goes down, and the Gaussian distribution becomes exponentially broader, reaching a variance of 24 nm for an annealing time of 30 s. The total fraction of counts in the lower and upper tails in fact increases with annealing time, consistent with broadening of the gaussian distribution (see Supplement 1). For annealing time shorter than 5 s, single centers were not observed as shown in Fig. 4(e). The increase in the statistical broadening is attributed to the introduction of defects during annealing such as vacancies [43]. The inhomogeneous broadening of single centers is always larger than the one observed for an ensemble of centers. The latter can be considered as the minimum broadening for the given carbon implantation condition since any other thermal annealing processing results in a larger inhomogeneous broadening. The mean value of the ZPL emission of single emitters is blue shifted as compared to the ZPL of the ensemble. The blue shift varies from 5 nm for 5 s annealing to approximately 10 nm for 30 s annealing. The ZPL wavelengths are well fitted by a Gaussian distribution shown by a solid red line in Fig. 4(a)-(d) (see Supplement 1).

3.4. *Ab-initio calculations of local strain effect*

It appears from the statistics of the ZPL emission wavelength of single centers that they are very sensitive to annealing. Annealing seems to change the local microscopic environment of the centers [44]. While the overall "blue-shift" can be understood from a macroscopic average strain, the large inhomogeneous broadening can only be explained by nanoscale processes that occur during annealing. To better understand these processes, we performed first-principles calculations of G-centers in silicon using the Vienna *ab initio* simulation package (VASP) [45–48]. Excited state calculations are performed using the constrained occupation method and are subsequently used to obtain the ZPL and PL spectra [36]. The G-center defect is embedded within a $3\times3\times3$ supercell of silicon containing 216 silicon atoms and simulated using the Heyd-Scuseria-Ernzerhof (HSE06) functional at the Γ-point [13,16,49]. In Fig. 5(a), we computed the photoluminescence spectra under strain while changing the lattice constant of the supercell in the *xy*-plane by -2% to 2% in increments of 1%. A full structural relaxation was performed alongside the electronic structure optimization to obtain the true defect ground state. It should also be noted that these calculations are subject to finite-size effects due to the limit of computational resources, such as the periodic boundary at the edge of the $3\times3\times3$ supercell and the elevated carbon concentration (~1 carbon per 100 silicon atoms) as compared to experiment (<1 carbon per 1000 silicon atoms).

Figure 5(a) shows that, as the lattice constant of the silicon supercell increases, the ZPL also increases in energy, corresponding to a "blue-shift" of the PL spectrum. For compressive strain, a "red-shift" of the ZPL is observed. For the same magnitude of strain, the shift of the ZPL is twice as large for tensile than for compressive strain. The asymmetry in the shift of the ZPL is illustrated in Fig. 5(b). The convexity of the shift vs strain plot suggests that blue shifts saturate at some point with increasing tensile strains and may explain why the blue shift is static after a short annealing time in Fig. 4(e). Since the supercell lattice in presence of a G-center is already under compression as compared to pristine silicon, further compression requires considerable energy and significantly impacts the electronic structure, while the effect of tensile strain is comparatively smaller. In the experiment, we measure the average ZPL emission from single centers to be blue shifted on average by about 10 nm, corresponding to a strain of $(\Delta a/a) \approx 0.3\%$.

Optics EXPRESS

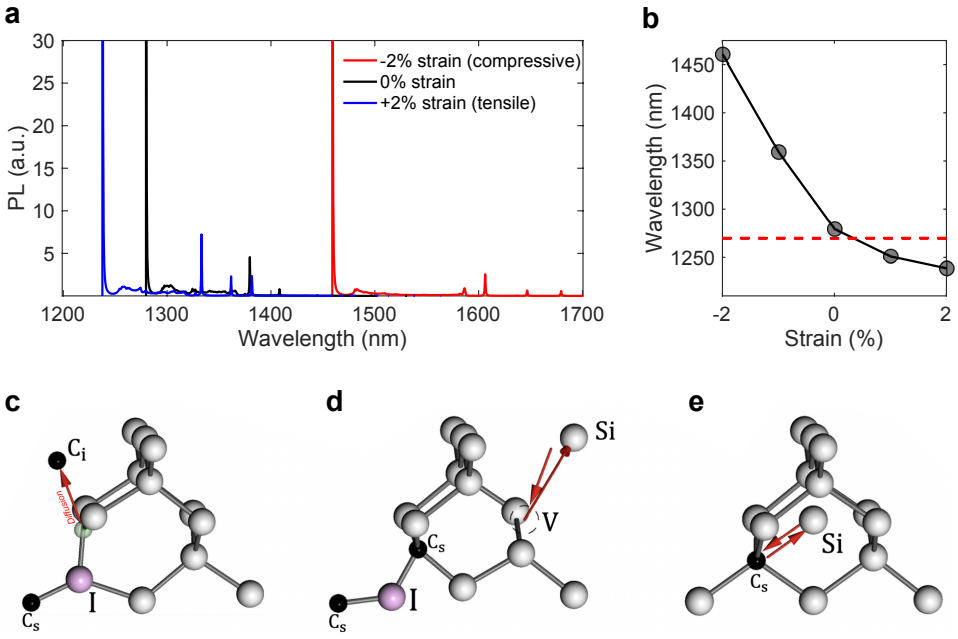

Fig. 5. Zero phonon line and photoluminescence spectra of the G-center strained in the *xy*-plane. (a) PL spectrum of G-center with -2% strain (red), + 2% strain (blue), and unstrained (black). All ZPLs are given relative to the experimental ZPL of the unstrained G-center. (b) ZPL of the G-center vs. strain, relative to the unstrained value. The red dashed line indicates the ZPL of a defect in a silicon sample annealed for 30s (1270 nm). The corresponding value of strain is equal to 0.335%. (c) Quenching of G-center defects in ensembles. (d) Formation of vacancies near a G-center. (e) Incorporation of carbon interstitials into substitutional lattice positions.

Annealing silicon results in several processes that can affect defect emission, including the decay of carbon interstitials, quenching of G-center defects in ensembles, and vacancies in the silicon lattice. These processes can result in local strain around the G-center, which we will now explore using first principles electronic structure calculations. In the first scenario (Fig. 5(c)), upon annealing the optically active B-type, with two substitutional carbons, can be converted to the dark A-type configuration in which one of the carbons moves to an interstitial position. This is possible because of the small energetic barrier between the A and B forms of the G-center (20 meV) [16,36]. The interconversion will be accompanied by the destruction of G-centers as the created $C_{(i)}$ decay (Fig. 5(c)). To compute the strain induced by this process, we placed two G-center defects inside a $3\times3\times3$ silicon supercell, and the atomic positions were relaxed while keeping the volume fixed by the experimental silicon lattice constant. The volume expands by 1.22% for the isolated G-center as compared to the volume in the presence of a nearby G-center within the supercell. The second possible process involves the formation of vacancies near a G-center (Fig. 5(d)). The creation of a vacancy is accompanied by the diffusion of a silicon atom away from its usual lattice position, becoming a self-interstitial. By introducing vacancies into a $3\times3\times3$ silicon supercell containing a G-center at a varying distance away from the defect, we find that this process tends to locally expand the lattice around the G-center by as much as 1 - 1.5% as compared to the unperturbed case (see Supplement 1). In the third process (Fig. 5(e)), a carbon interstitial can decay by incorporating into the silicon lattice as a substitutional carbon, simultaneously creating a silicon self-interstitial. We investigate the effect of this process by simulating two systems: 1) a $3\times3\times3$ silicon supercell containing a single carbon interstitial, and

Optics EXPRESS

2) a supercell with one substitutional carbon and one adjacent silicon self-interstitial. Performing a complete relaxation of the atomic positions and unit cell volume, we find that the volume of the latter is smaller by 0.330%. In the three processes discussed above, the silicon lattice locally contracts by a percent or less causing a compensating expansion around the G-center and explaining the overall "blue-shift" of the emission. Moreover, the magnitude of the induced local strain is highly dependent on the distance between the G-center and the location of the microscopic process causing the strain (see Supplement 1). We notice that the strain can vary from -0.5% to 1% depending on the location of the vacancy and may cause the observed large inhomogeneous broadening in the emission of single centers.

4. Conclusion

We investigated the effect of rapid thermal annealing on the formation and spectral properties of single centers in silicon. Rapid thermal annealing is necessary for the formation of single centers with high signal to background ratio in carbon implanted samples. The annealing time is found to be a parameter to control the inhomogeneous broadeningannealing and density of defects in silicon on insulator wafers annealed for a short time. We identified an annealing time window for single center formation below which only an ensemble of centers exists and beyond which all single centers are destroyed. We also found that annealing, while important for forming single centers, creates a fluctuation in their properties such as their zero phonon lines and the fluctuation was attributed to local strain variations induced by microscopic processes during annealing. Annealing thus appears to currently be the limiting factor for the scalable manufacturing of single centers in silicon and calls for color center formation methods not involving the annealing step such as implanting with lower doses.

Funding. National Science Foundation (OMA-2016245, QuIC-TAQS 2137645); Gordon and Betty Moore Foundation (The Moore Inventor Fellows programme); U.S. Department of Energy (DE-AC02-05CH11231, DE-NA-003525).

Acknowledgment. This research used resources of the National Energy Research Scientific Computing Center, a DOE Office of Science User Facility supported by the Office of Science of the U.S. Department of Energy under Contract No. DE-AC02-05CH11231.

Disclosures. The authors declare no competing interests.

Data availability. The data that support the findings of this study are available from the corresponding author upon reasonable request.

Supplemental document. See Supplement 1 for supporting content.

References

1. R. E. Camacho-Aguilera, Y. Cai, N. Patel, J. T. Bessette, M. Romagnoli, L. C. Kimerling, and J. Michel, "An electrically pumped germanium laser," Opt. Express **20**(10), 11316–11320 (2012).
2. S.-L. Cheng, J. Lu, G. Shambat, H.-Y. Yu, K. Saraswat, J. Vuckovic, and Y. Nishi, "Room temperature 1.6 μm electroluminescence from Ge light emitting diode on Si substrate," Opt. Express **17**(12), 10019–10024 (2009).
3. J. R. Jain, A. Hryciw, T. M. Baer, D. A. B. Miller, M. L. Brongersma, and R. T. Howe, "A micromachining-based technology for enhancing germanium light emission via tensile strain," Nat. Photonics **6**(6), 398–405 (2012).
4. J. R. Sánchez-Pérez, C. Boztug, F. Chen, F. F. Sudradjat, D. M. Paskiewicz, R. B. Jacobson, M. G. Lagally, and R. Paiella, "Direct-bandgap light-emitting germanium in tensilely strained nanomembranes," Proc. Natl. Acad. Sci. **108**(47), 18893–18898 (2011).
5. X. Sun, J. Liu, L. C. Kimerling, and J. Michel, "Room-temperature direct bandgap electroluminesence from Ge-on-Si light-emitting diodes," Opt. Lett. **34**(8), 1198–1200 (2009).
6. D. J. Lockwood, "Chapter 1 Light Emission in Silicon," in *Light Emission in Silicon: From Physics to Devices*, 49, D. J. Lockwood, Ed. (Elsevier, 1997), pp. 1–35.
7. E. F. Schubert, *Doping in III-V Semiconductors* (Cambridge University Press, 1993).
8. R. A. Levy, *Microelectronic Material and Processes* (Springer Dordrecht, 1989).
9. I. Aharonovich, D. Englund, and M. Toth, "Solid-state single-photon emitters," Nat. Photonics **10**(10), 631–641 (2016).
10. N. Kalb, A. A. Reiserer, P. C. Humphreys, J. J. W. Bakermans, S. J. Kamerling, N. H. Nickerson, S. C. Benjamin, D. J. Twitchen, M. Markham, and R. Hanson, "Entanglement distillation between solid-state quantum network nodes," Science **356**(6341), 928–932 (2017).

Optics EXPRESS

11. R. J. Spry and W. D. Compton, "Recombination Luminescence in Irradiated Silicon," Phys. Rev. **175**(3), 1010–1020 (1968).
12. R. B. Capaz, A. Dal Pino, and J. D. Joannopoulos, "Theory of carbon-carbon pairs in silicon," Phys. Rev. B **58**(15), 9845–9850 (1998).
13. H. Wang, A. Chroneos, C. A. Londos, E. N. Sgourou, and U. Schwingenschlögl, "G-centers in irradiated silicon revisited: A screened hybrid density functional theory approach," J. Appl. Phys. **115**(18), 183509 (2014).
14. A. Mattoni, F. Bernardini, and L. Colombo, "Self-interstitial trapping by carbon complexes in crystalline silicon," Phys. Rev. B **66**(19), 195214 (2002).
15. M. S. Potsidi and C. A. Londos, "The CiCs(SiI) defect in silicon: An infrared spectroscopy study," J. Appl. Phys. **100**(3), 033523 (2006).
16. L. W. Song, X. D. Zhan, B. W. Benson, and G. D. Watkins, "Bistable interstitial-carbon–substitutional-carbon pair in silicon," Phys. Rev. B **42**(9), 5765–5783 (1990).
17. G. Davies, "The optical properties of luminescence centres in silicon," Phys. Rep. **176**(3-4), 83–188 (1989).
18. P. Udvarhelyi, B. Somogyi, G. Thiering, and A. Gali, "Identification of a Telecom Wavelength Single Photon Emitter in Silicon," Phys. Rev. Lett. **127**(19), 196402 (2021).
19. O. O. Awadelkarim, A. Henry, B. Monemar, J. L. Lindström, Y. Zhang, and J. W. Corbett, "Photoluminescence study of radiative channels in ion-implanted silicon," Phys. Rev. B **42**(9), 5635–5640 (1990).
20. G. Davies, E. C. Lightowlers, M. F. Thomaz, and J. G. Wilkes, "A metastable precursor to the production of the two-carbon-atom 'G' centre in irradiated crystalline silicon," Semicond. Sci. Technol. **3**(6), 608–611 (1988).
21. W. Redjem, A. Durand, T. Herzig, A. Benali, S. Pezzagna, J. Meijer, A. Y. Kuznetsov, H. S. Nguyen, S. Cueff, J. M. Gérard, I. Robert-Philip, B. Gil, D. Caliste, P. Pochet, M. Abbarchi, V. Jacques, A. Dréau, and G. Cassabois, "Single artificial atoms in silicon emitting at telecom wavelengths," Nat. Electron. **3**(12), 738–743 (2020).
22. M. Hollenbach, Y. Berencén, U. Kentsch, M. Helm, and G. V. Astakhov, "Engineering telecom single-photon emitters in silicon for scalable quantum photonics," Opt. Express **28**(18), 26111–26121 (2020).
23. C. Beaufils, W. Redjem, E. Rousseau, V. Jacques, A. Y. Kuznetsov, C. Raynaud, C. Voisin, A. Benali, T. Herzig, S. Pezzagna, J. Meijer, M. Abbarchi, and G. Cassabois, "Optical properties of an ensemble of G-centers in silicon," Phys. Rev. B **97**(3), 035303 (2018).
24. A. Durand, Y. Baron, W. Redjem, T. Herzig, A. Benali, S. Pezzagna, J. Meijer, A. Y. Kuznetsov, J.-M. Gérard, I. Robert-Philip, M. Abbarchi, V. Jacques, G. Cassabois, and A. Dréau, "Broad Diversity of Near-Infrared Single-Photon Emitters in Silicon," Phys. Rev. Lett. **126**(8), 083602 (2021).
25. Y. Baron, A. Durand, P. Udvarhelyi, T. Herzig, M. Khoury, S. Pezzagna, J. Meijer, I. Robert-Philip, M. Abbarchi, J.-M. Hartmann, V. Mazzocchi, J.-M. Gérard, A. Gali, V. Jacques, G. Cassabois, and A. Dréau, "Detection of Single W-Centers in Silicon," ACS Photonics **9**(7), 2337–2345 (2022).
26. D. B. Higginbottom, A. T. K. Kurkjian, and C. Chartrand, *et al.*, "Optical observation of single spins in silicon," Nature **607**(7918), 266–270 (2022).
27. M. Prabhu, C. Errando-Herranz, L. D. Santis, I. Christen, C. Chen, and D. Englund, "Individually Addressable Artificial Atoms in Silicon Photonics," arXiv, arXiv:2202.02342 (2022).
28. R. Contractor, W. Noh, and W. Redjem, *et al.*, "Scalable single-mode surface-emitting laser via open-Dirac singularities," Nature **608**(7924), 692–698 (2022).
29. M. Hollenbach, N. Klingner, and N.S. Jagtap, *et al.*, "Wafer-scale nanofabrication of telecom single-photon emitters in silicon," Nat. Commun. **13**(1), 7683 (2022).
30. C. Chartrand, L. Bergeron, K. J. Morse, H. Riemann, N. V. Abrosimov, P. Becker, H.-J. Pohl, S. Simmons, and M. L. W. Thewalt, "Highly enriched 28Si reveals remarkable optical linewidths and fine structure for well-known damage centers," Phys. Rev. B **98**(19), 195201 (2018).
31. B. Kambs and C. Becher, "Limitations on the indistinguishability of photons from remote solid state sources," New J. Phys. **20**(11), 115003 (2018).
32. N. A. Sobolev, A. E. Kalyadin, E. I. Shek, V. I. Sakharov, I. T. Serenkov, V. I. Vdovin, E. O. Parshin, and M. I. Makoviichuk, "Photoluminescence in silicon implanted with erbium ions at an elevated temperature," Phys. Status Solidi C **45**(8), 1006–1008 (2011).
33. D. Korolev, A. Mikhaylov, A. Belov, and D. Tetelbaum, "Effect of intrinsic impurities and annealing conditions on dislocation-related luminescence in self-ion-implanted Si," Phys. Status Solidi C **13**(10-12), 937–939 (2016).
34. S. A. Campbell, *The science and engineering of microelectronic fabrication*, vol. 164 (Oxford University Press, 2001).
35. R. C. Newman and J. Wakefield, "The diffusivity of carbon in silicon," J. Phys. Chem. Solids **19**(3-4), 230–234 (1961).
36. V. Ivanov, J. Simoni, Y. Lee, W. Liu, K. Jhuria, W. Redjem, Y. Zhiyenbayev, C. Papapanos, W. Qarony, B. Kanté, A. Persaud, T. Schenkel, and L. Z. Tan, "Effect of localization on photoluminescence and zero-field splitting of silicon color centers," Phys. Rev. B **106**(13), 134107 (2022).
37. W. Redjem, A. J. Amsellem, and F. I. Allen, *et al.*, "Defect engineering of silicon with ion pulses from laser acceleration," arXiv, arXiv:2203.13781 (2022).
38. R. Brouri, A. Beveratos, J.-P. Poizat, and P. Grangier, "Photon antibunching in the fluorescence of individual color centers in diamond," Opt. Lett. **25**(17), 1294–1296 (2000).

Optics EXPRESS

39. M. Suezawa, Y. Iijima, and I. Yonenaga, "Vacancy- and interstitial-mediated self-diffusion coefficients determined from the analysis of observed self-diffusion coefficients in silicon crystals," Jpn. J. Appl. Phys. **59**(4), 045505 (2020).
40. E. S. Johnson, W. D. Compton, J. R. Noonan, and B. G. Streetman, "Recombination luminescence from electron-irradiated Li-diffused Si," J. Appl. Phys. **44**(12), 5411–5418 (1973).
41. R. B. Capaz, A. Dal Pino, and J. D. Joannopoulos, "Identification of the migration path of interstitial carbon in silicon," Phys. Rev. B **50**(11), 7439–7442 (1994).
42. F. Mechighel, N. Armour, and S. Dost, "Modeling of the effect of the presence of a free surface on transport structures and mixing during the dissolution process of silicon into germanium melt," J. Therm. Anal. Calorim. **146**(1), 61–91 (2021).
43. T. A. Frewen and T. Sinno, "Vacancy self-trapping during rapid thermal annealing of silicon wafers," Appl. Phys. Lett. **89**(19), 191903 (2006).
44. V. D. Tkachev and A. V. Mudryi, "Piezospectroscopic effect on zero-phonon luminescence lines of silicon," J. Appl. Spectrosc. **29**(6), 1485–1491 (1978).
45. G. Kresse and J. Hafner, "Ab initio molecular dynamics for liquid metals," Phys. Rev. B **47**(1), 558–561 (1993).
46. G. Kresse and J. Hafner, "Ab initio molecular-dynamics simulation of the liquid-metal–amorphous-semiconductor transition in germanium," Phys. Rev. B **49**(20), 14251–14269 (1994).
47. G. Kresse and J. Furthmüller, "Efficiency of ab-initio total energy calculations for metals and semiconductors using a plane-wave basis set," Comput. Mater. Sci. **6**(1), 15–50 (1996).
48. G. Kresse and J. Furthmüller, "Efficient iterative schemes for ab initio total-energy calculations using a plane-wave basis set," Phys. Rev. B **54**(16), 11169–11186 (1996).
49. A. V. Krukau, O. A. Vydrov, A. F. Izmaylov, and G. E. Scuseria, "Influence of the exchange screening parameter on the performance of screened hybrid functionals," J. Chem. Phys. **125**(22), 224106 (2006).